JACS Au
AN OPEN ACCESS JOURNAL OF THE AMERICAN CHEMICAL SOCIETY

pubs.acs.org/jacsau

Article

Mobility and Reactivity of Cu^+ Species in Cu-CHA Catalysts under NH_3-SCR-NOx Reaction Conditions: Insights from AIMD Simulations

Reisel Millan, Pieter Cnudde, Veronique van Speybroeck,* and Mercedes Boronat*

Cite This: *JACS Au* 2021, 1, 1778–1787

Read Online

ACCESS | Metrics & More | Article Recommendations | Supporting Information

ABSTRACT: The mobility of the copper cations acting as active sites for the selective catalytic reduction of nitrogen oxides with ammonia in Cu-CHA catalysts varies with temperature and feed composition. Herein, the migration of $[Cu(NH_3)_2]^+$ complexes between two adjacent cavities of the chabazite structure, including other reactant molecules (NO, O_2, H_2O, and NH_3), in the initial and final cavities is investigated using ab initio molecular dynamics (AIMD) simulations combined with enhanced sampling techniques to describe hopping events from one cage to the other. We find that such diffusion is only significantly hindered by the presence of excess NH_3 or NO in the initial cavity, since both reactants form with $[Cu(NH_3)_2]^+$ stable intermediates which are too bulky to cross the 8-ring windows connecting the cavities. The presence of O_2 modifies strongly the interaction of NO with Cu^+. At low temperatures, we observe NO detachment from Cu^+ and increased mobility of the $[Cu(NH_3)_2]^+$ complex, while at high temperatures, NO reacts spontaneously with O_2 to form NO_2. The present simulations give evidence for recent experimental observations, namely, an NH_3 inhibition effect on the SCR reaction at low temperatures, and transport limitations of NO and NH_3 at high temperatures. Our first principle simulations mimicking operating conditions support the existence of two different reaction mechanisms operating at low and high temperatures, the former involving dimeric $Cu(NH_3)_2$-O_2-$Cu(NH_3)_2$ species and the latter occurring by direct NO oxidation to NO_2 in one single cavity.

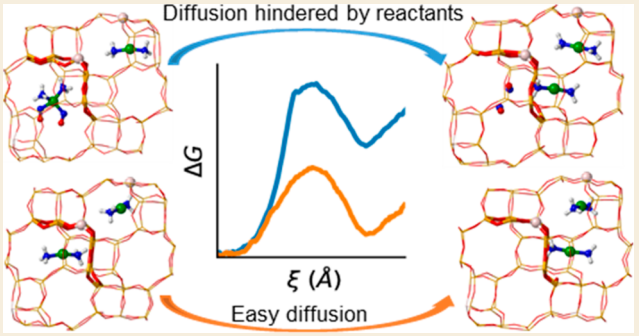

KEYWORDS: *zeolite, molecular dynamics, cation mobility, DFT, mechanism*

1. INTRODUCTION

One of the most efficient technologies to remove nitrogen oxides (NO_x) emissions from stationary power plants and diesel vehicles is the selective catalytic reduction (SCR) reaction using ammonia as a reducing agent (NH_3-SCR-NOx).[1−3] The catalysts currently employed in transport applications are copper−exchanged zeolites, in particular, those possessing small-pore structures such as LTA, AEI, and CHA.[4−9] The reaction of NO and NH_3 in the presence of O_2 according to the standard SCR reaction (eq 1) or with NO_2 in the fast SCR reaction (eq 2) produces harmless and nonpolluting N_2 and H_2O

$$4NH_3 + 4NO + O_2 \rightarrow 4N_2 + 6H_2O \quad (1)$$

$$4NH_3 + 2NO + 2NO_2 \rightarrow 4N_2 + 6H_2O \quad (2)$$

The experimental and theoretical research effort devoted in the past decade to understand the NH_3-SCR-NOx reaction mechanism has established some key points of this complex process.[10−18] There is general consensus that the mechanism consists of a Cu^+/Cu^{2+} redox cycle comprising an oxidation step in which Cu^+ is oxidized to Cu^{2+} by NO_2 (fast SCR) or by reaction of NO + O_2 (standard SCR), and a reduction step of Cu^{2+} to Cu^+ with the simultaneous participation of NH_3 and NO (Scheme 1). It is also accepted that Brønsted acid sites play a role in the decomposition of nitrite and nitrate intermediates formed in the oxidation half-cycle, and in the transformation of the nitrosamine NH_2NO molecule generated in the reduction step into N_2 and H_2O.[17−20] However, there is

Scheme 1. Schematic Representation of NH_3-SCR-NOx Catalytic Cycle

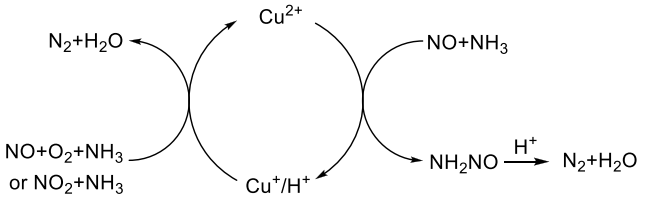

Received: July 31, 2021
Published: September 17, 2021

still some uncertainty regarding the location, molecular environment, and mobility of the catalytically active Cu^+ and Cu^{2+} species under reaction conditions, and especially on how changes in temperature and feed composition affect the dynamic nature of the active sites. Operando X-ray absorption and emission spectroscopic (XAS/XES) studies have shown that at low temperatures (T < 473 K) and in the presence of NH_3, Cu^+ and Cu^{2+} cations exist preferentially as mobile $[Cu(NH_3)_2]^+$ and $[Cu(NH_3)_4]^{2+}$ species. At higher temperatures (T > 523 K), the Cu-complexes are expected to lose their ligands and again occupy positions in the 6-ring or 8-ring windows of the zeolite structure, directly coordinated to the framework oxygen atoms, forming a true heterogeneous single-site catalyst. This restructuring of the active sites leads to a decrease in the catalytic activity between 573 and 623 K, together with a change in the operating reaction mechanism reflected in an increase in the apparent activation energies from 70 kJ/mol at 473 K to 140 kJ/mol at 623 K.[9,19,21−30]

Focusing first on the low temperature regime, where the catalyst active sites exist predominantly as mobile $[Cu(NH_3)_2]^+$ and $[Cu(NH_3)_4]^{2+}$ complexes confined within the chabazite cavities, the oxidation of Cu^+ to Cu^{2+} occurs through the formation of transient dimeric $Cu(NH_3)_2$-O_2-$Cu(NH_3)_2$ species that have been very recently observed experimentally by UV−vis spectroscopy.[31,32] According to this mechanistic proposal, the diffusion of the $[Cu(NH_3)_2]^+$ monomers through the 8-ring windows of the chabazite structure to form dimers is the rate-determining step of the process, which explains the second-order dependence of the SCR reaction rate with Cu density at low temperature.[12−18] Activation energy barriers of 35 and 37 kJ/mol were estimated from static DFT calculations for the migration of one $[Cu(NH_3)_2]^+$ monomer into an adjacent cavity, either completely empty[12] or occupied by just another $[Cu(NH_3)_2]^+$ monomer.[14] These rather low values would suggest that crossing the 8-ring window is easy. However, the diffusion of chemical species within a zeolite catalyst may be largely affected, not only by the working conditions, such as operating temperature, but also especially by other reactive species present inside the zeolite microporous structure.

In this sense, an NH_3 inhibition effect on the SCR reaction has been identified at low temperatures by different groups using *in situ* and *operando* XAS techniques combined with catalytic activity tests. This inhibition effect has been specifically attributed to a decrease in the rate of the oxidation step ($Cu^+ \rightarrow Cu^{2+}$) due to the high stability of NH_3 solvated $[Cu(NH_3)_x]^+$ species.[26,27,29,30] With increasing temperature, the NH_3 solvation sphere of copper cations is partly lost, leading to a higher proportion of Cu^+ and Cu^{2+} cations directly coordinated to the zeolite framework, while the conversion of NO is significantly enhanced.[26,27,29] The improved catalytic activity at T > 623 K has been tentatively attributed to (i) a deficit of NH_3 that is consumed in the parallel NH_3 oxidation reaction thus diminishing the inhibition effect and (ii) to the onset of NO oxidation to NO_2 which would participate in the fast SCR reaction (eq 2) thus boosting the reaction rate.[27,29,33] In addition, a recent study combining *operando* XANES with microtomography and catalyst testing reports spatial gradients in the oxidation state of copper under high temperature reaction conditions, which are attributed to mass transport limitations of NH_3 and NO to the inner regions of the zeolite catalyst.[30]

All these experimental results strongly evidence the key role of other reactants on the mobility and reactivity of the copper cations acting as active sites for the SCR reaction, and put forward the need to take into account these species in realistic simulations at operating conditions. To capture such effects, some of us recently proposed a first principle based molecular dynamics approach combined with enhanced sampling techniques to estimate free energy diffusion barriers in complex molecular environments, taking into account true loadings with other species at various temperatures.[34] The methodology has been successfully applied to the study of hydrocarbon diffusion in the context of the methanol-to-olefins process.[35,36] Especially for the SCR process, the effect of temperature and the interactions of the $[Cu(NH_3)_2]^+$ complexes with other molecules present in the cavities may greatly modify the mobility of reactive species. Using regular ab initio molecular dynamics (AIMD) simulations in combination with *in situ* IR spectroscopy, we recently studied the interaction of Cu-CHA catalysts with reactants and intermediates of the NH_3-SCR-NOx reaction at realistic reaction conditions.[37] We showed that in the low temperature regime, NH_3 is able to release Cu^+ cations from their positions coordinated to the zeolite framework forming $[Cu(NH_3)_2]^+$ complexes that migrate to the center of the cavity and, eventually, cross to an adjacent empty cavity. However, in our previous study, we did not study transport properties through the 8-membered ring, as hopping from one cage to the other is a rare event and therefore enhanced sampling techniques such as umbrella sampling, metadynamics, etc., need to be used.[34−36] In this work, we intend to unveil key aspects of the oxidation half-cycle of the SCR mechanism at low (T < 473 K) and high (T > 523 K) temperature by means of enhanced sampling molecular dynamics simulations under operating conditions. First, we study the diffusion of $[Cu(NH_3)_2]^+$ monomers, necessary to form the dimers involved in the activation of molecular O_2 at low temperature, in catalyst models with a molecular environment representative of the actual SCR reaction conditions. For this purpose, we use AIMD simulations in combination with umbrella sampling (US), to extract Gibbs free energy profiles for the diffusion of $[Cu(NH_3)_2]^+$ complexes through the 8-ring windows of Cu-CHA in the presence of other reactant molecules, namely, NO, O_2, H_2O, and NH_3, at a temperature of 423 K representative of the low temperature regime. Second, the thermal stability of bulky $[Cu(NH_3)_2]^+(NO)_x$ complexes, relevant to understand the experimentally reported mass transport limitations of NH_3 and NO, is investigated by means of regular MD simulations at increasing temperature: 298, 523, and 673 K. Finally, the formation of NO_2 by direct NO oxidation with O_2 in the presence of a $[Cu(NH_3)_2]^+$monomer is explored at high (673 K) and low (423 K) temperature to assess the possible contribution of the fast SCR reaction (eq 2) to the global catalytic cycle at high and low temperatures. The present theoretical study provides new insights into the mobility and reactivity of $[Cu(NH_3)_2]^+$species in Cu-CHA catalysts under different reaction conditions explicitly accounting for other reacting species present in the pores of the zeolites.

2. COMPUTATIONAL DETAILS

The Cu-CHA catalyst was modeled by means of a hexagonal unit cell containing 2 Al, 34 Si, and 72 O atoms, with only two exceptions described below. In the simulations of the low temperature diffusion of $[Cu(NH_3)_2]^+$ species through the 8-

https://doi.org/10.1021/jacsau.1c00337
JACS Au 2021, 1, 1778−1787

ring windows of CHA, the two Al atoms were placed in adjacent cavities, separated by a distance of 8.6 Å as depicted in Figure S1a, and the net negative charge generated in the framework was compensated by two $[Cu(NH_3)_2]^+$ complexes initially placed in adjacent cavities. This Al distribution leads to stable $[Cu(NH_3)_2]^+$ pairs in Cu-CHA.[38] A model with one Al and 35 Si atoms was used to investigate the diffusion of one $[Cu(NH_3)_2]^+$ monomer to an adjacent empty cavity (Figure 1a), while a larger 1 × 2 × 1 unit cell containing 1 Al, 71 Si, and 144 O atoms was used to model the diffusion of $[Cu(NH_3)_2]^+$ at larger distances from the charge compensating Al site (Figure S1b). While the Si/Al ratio of the models used (17, 35, and 71) is higher than that of the real catalysts employed for this reaction, ∼10, all models are equivalent in that they contain one Al in the 8-ring window through which the $[Cu(NH_3)_2]^+$ complex diffuses and, as shown later, the barrier for diffusion of one isolated $[Cu(NH_3)_2]^+$changes by less than 5 kJ/mol when the Si/Al ratio increases from 35 to 71. To study the thermal stability of bulky $[Cu(NH_3)_2]^+(NO)_x$ complexes by means of regular MD simulations at increasing temperature and to obtain the Gibbs free energy profile for the NO oxidation reaction at 423 K, we used the same catalyst model previously employed to investigate the mobility of copper cations under reaction conditions in ref 37. In this model, the two Al were located in the same 6-ring, separated by one framework Si atom, and the two negative charges generated by this substitution were compensated with one H^+ attached to a framework O and one Cu^+ ion placed in the 6-ring plane (see Figure S1c in the SI).

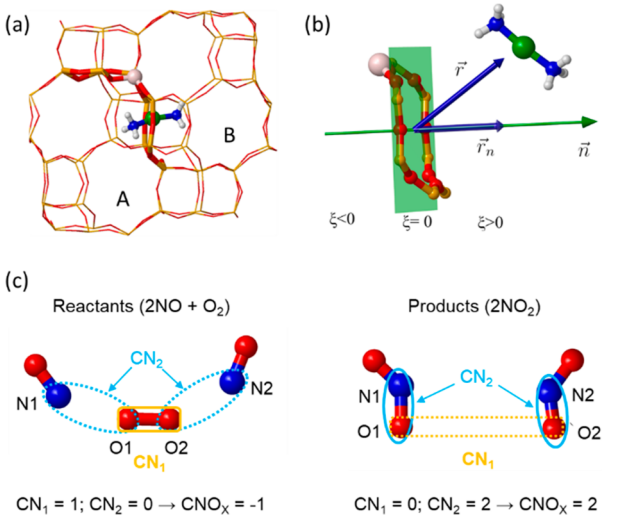

Figure 1. (a) Diffusion of $[Cu(NH_3)_2]^+$ complex from cavity A (ξ < 0) to cavity B (ξ > 0). (b) Representation of the collective variable ξ describing $[Cu(NH_3)_2]^+$ diffusion through the 8-ring window (green plane). (c)) Representation of the coordination numbers CN_1, CN_2, and CN_{OX} before (left) and after (right) the reaction. Si, O, Al, Cu, N, and H atoms are depicted in yellow, red, thatch, green, blue, and white, respectively.

All AIMD simulations were performed with the CP2K package[39] at the revPBE-D3[40,41] level of theory. The Gaussian and Plane Waves (GPW) method[42] was used with the TZVP basis set for all atoms except Cu, which was described with the DZVP-MOLOPT-SR-GTH basis set. A cutoff energy of 400 Ry was used for the auxiliary plane waves. Core electrons were represented with GTH pseudopotentials.[43] Regular AIMD simulations were run in the NPT ensemble consisting of a production run of 50 ps after 10 ps of equilibration. Three temperatures were considered, 298, 523, and 673 K, controlled by a Nosé−Hoover chain thermostat[44,45] with three beads and a time constant of 300 fs. The pressure in the NPT simulations was set to 1 atm, controlled by a Martyna-Tobias-Klein barostat.[46] The time step to integrate the equations of motion was set to 0.5 fs.

Gibbs free energy profiles for the diffusion of the $[Cu(NH_3)_2]^+$ species through the 8-ring windows of Cu-SSZ-13 zeolite and for the oxidation of NO to NO_2 were obtained from ab initio umbrella sampling (AI-US) simulations[47] at 423 K. In order to calculate a free energy profile with the AI-US technique, it is necessary first to define a collective variable that unambiguously represents the process considered. According to our earlier work,[34] the collective variable (ξ) that best describes the diffusion of $[Cu(NH_3)_2]^+$ from a cavity A (ξ < 0) to a cavity B (ξ > 0) (see Figure 1a) is the projection of the position vector of the Cu atom on the vector normal to the average plane of the 8-ring, with the value ξ = 0 corresponding to Cu placed in the plane of the 8-ring (see Figure 1b).

To describe the $2NO + O_2 \rightarrow 2NO_2$ reaction at 423 K, a collective variable (CN_{OX}) was defined that represents the simultaneous dissociation of the O−O bond of O_2 and the formation of two new N−O bonds. Two coordination numbers tracking the coordination of the O atoms of the O_2 molecule with each other (CN_1) and with the N atoms of the NO molecules (CN_2) were defined as follows

$$CN = \sum_{i,j} \frac{1 - (r_{ij}/r_0)^m}{1 - (r_{ij}/r_0)^n}$$

where r_{ij} is the distance between atom i and atom j, r_0 is a switching cutoff distance that defines interatomic contact, and m and n are exponents, set to 6 and 12, respectively, in such a way that each term of the summation equals 0.5 for $r_{ij} = r_0$ and decays exponentially to 0 for larger values of r_{ij}. The r_0 values for CN_1 and CN_2 are 1.6 and 2.0 Å, respectively. The collective variable $CN_{OX} = CN_2 - CN_1$, so that it ranges from −1 in the initial state ($2NO+O_2$) to 2 in the final state ($2NO_2$) (see Figure 1c).

In the AI-US simulations, the collective variable was split into at least 40 equidistant windows. For each window, an independent biased AIMD simulation was carried out restricting the collective variable to one specific value but ensuring complete sampling of the configuration space in all other degrees of freedom. This method ensures that all points along the diffusion path are sampled equally well,[48] although at a high computational cost. In each window, an independent MD simulation of 10 ps is run, leading to a total of 400 ps time for each AI-US simulation. A harmonic bias potential centered at the corresponding value of the collective variable was applied to restrict the sampling to each window individually and to ensure sufficient overlap between the sampling of adjacent windows. The force constant of the harmonic potential was set to 50 kJ/mol/Å^2 for collective variable ξ and to 50 kJ/mol for collective variable CN_{OX}. No additional walls were imposed and in this sense all other molecules present (NO, O_2, H_2O and NH_3) were free to move out of their original cavities. All AI-US simulations were performed with PLUMED 2.5[49] interfaced to the CP2K engine and consisted in a production run of 10 ps in the NPT ensemble

https://doi.org/10.1021/jacsau.1c00337
JACS Au 2021, 1, 1778−1787

for each window, after which sufficient overlap between adjacent windows was observed (Figures S2−S6). The samplings obtained in each window were then analyzed together using the weighted histogram analysis method (WHAM)[50,51] out of which the free energy profiles were generated.

3. RESULTS AND DISCUSSION

3.1. Diffusion of $[Cu(NH_3)_2]^+$ through the 8-Ring Window

In a first step, we investigated the diffusion of a single $[Cu(NH_3)_2]^+$ complex from one cavity A to an empty adjacent cavity B at 423 K. The hexagonal unit cell used in this case to model the Cu-CHA catalyst contains one Al atom placed between the two adjacent cavities A and B visited by the $[Cu(NH_3)_2]^+$ complex during the simulations (see Figure 1a). The activation free energy for the diffusion of $[Cu(NH_3)_2]^+$ to an empty cavity at 423 K is only 17 kJ/mol, and the process is thermoneutral (see case *I* in Table 1 and Figures 2 and 3).

Table 1. Activation Free Energies (ΔG_{act}) at Corresponding Values of Collective Variable (ξ_{act}), and Reaction Free Energies (ΔG_r) at Corresponding Collective Variable (ξr) for Diffusion of $Cu^+(NH_3)_2$ through *8r* Window of Cu-CHA at 423 K

	Cavity A	Cavity B	ΔG_{act}[a]	ΔGr[a]	ξ_{act}	ξr
I	Cu[b]		17	1.5	0.35	2.40
II	Cu	Cu	28	7	0.30	2.45
III	Cu	Cu + O_2	26	5	0.40	2.60
IV	Cu	Cu + 2NO + O_2	24	0	0.20	2.85
V	Cu + H_2O	Cu + H_2O	22	10	0.67	2.30
VI	Cu + NH_3	Cu + NH_3	28	15	0.90	2.40
VII	Cu + 2NH_3	Cu	47	36	1.04	2.30
VIII	Cu + 2NO	Cu	54	34	0.50	2.40

[a]ΔG_{act} and ΔGr in kJ/mol. [b]Cu represents the $[Cu(NH_3)_2]^+$ complex.

Using a larger 1 × 2 × 1 unit cell to model the catalyst, the diffusion to a third cavity C was also investigated (see Figure 4). The activation free energy necessary to cross the first 8-ring is 22 kJ/mol, similar to that found using the 1 × 1 × 1 unit cell, 17 kJ/mol. But as the $[Cu(NH_3)_2]^+$ complex moves away from cavity A, the free energy increases continuously and a second maximum at ξ = 8.4 is reached, corresponding to diffusion through the 8-ring window connecting cavities B and C, with a calculated activation free energy barrier of 76 kJ/mol. The high destabilization of the system as the $[Cu(NH_3)_2]^+$ complex migrates to cavities B and C is clearly associated with the weakening of the electrostatic interaction between the positively charged $[Cu(NH_3)_2]^+$ species and the negatively charged framework around the Al atom, located in the 8-ring connecting cavities A and B (see Figure 4).

The part of this profile corresponding to the diffusion of $[Cu(NH_3)_2]^+$ through the 8-ring not containing Al (diffusion from cavity B to cavity C in Figure 4) is in qualitative agreement with previous results from Paolucci et al.[14] They obtained a ∼20 kJ/mol lower free energy barrier for this step using a different enhanced sampling method, namely, metadynamics simulations, at a slightly higher temperature, 473 K, and where the Cu−Al distance was used as collective variable. As shown in the work of Bailleul et al.,[48] direct comparison of free energy profiles obtained along different collective variables is not possible, and first a proper coordinate transformation needs to be performed. Despite direct quantitative comparison is not possible due to the different

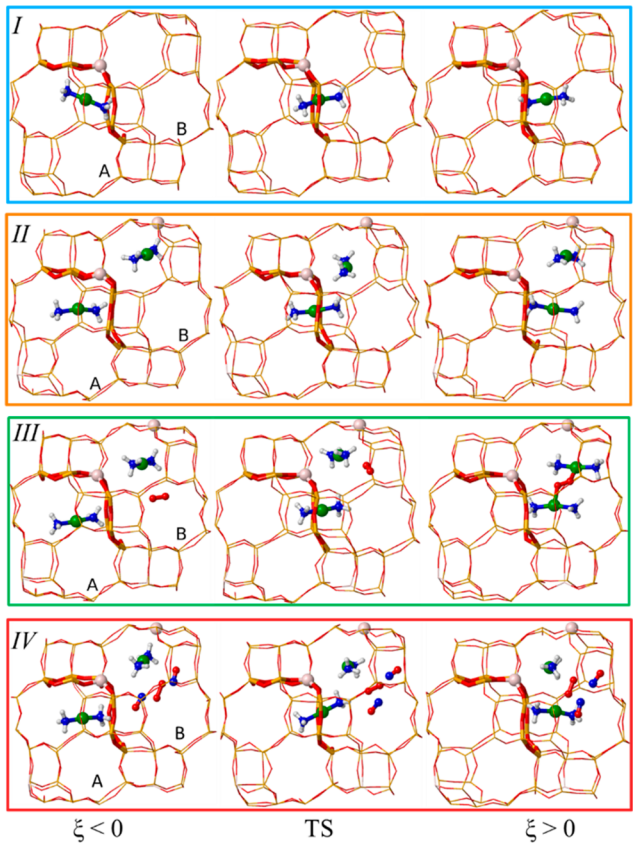

Figure 2. Snapshots of initial (ξ < 0), transition state (TS, ξ = 0) and final state (ξ > 0) of $[Cu(NH_3)_2]^+$ diffusion through the 8-ring windows of Cu-CHA at 423 K, in absence of other reactants and in the presence of O_2 and O_2+NO in cavity B. Si and O atoms in the framework are depicted as yellow and red sticks; Al, Cu, O in molecules and N and H atoms are depicted as thatch, green, red, blue, and white balls, respectively.

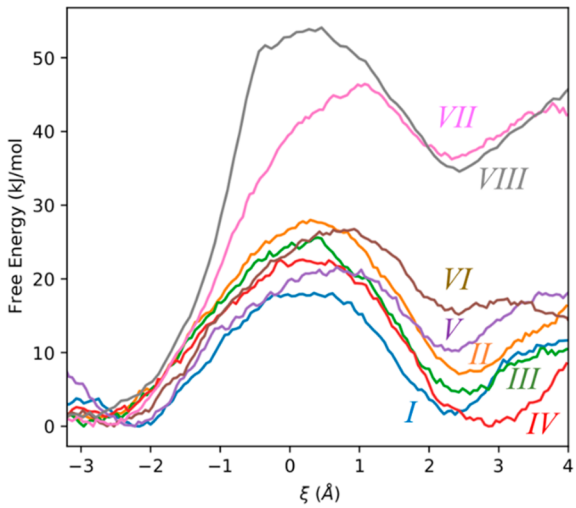

Figure 3. Free energy profiles for the diffusion of $Cu^+(NH_3)_2$ through the 8-ring windows of Cu-CHA from umbrella sampling AIMD simulations at 423 K. The labels correspond to cases *I*−*VIII* in Table 1 and Figures 2 and 5

https://doi.org/10.1021/jacsau.1c00337
JACS Au 2021, 1, 1778−1787

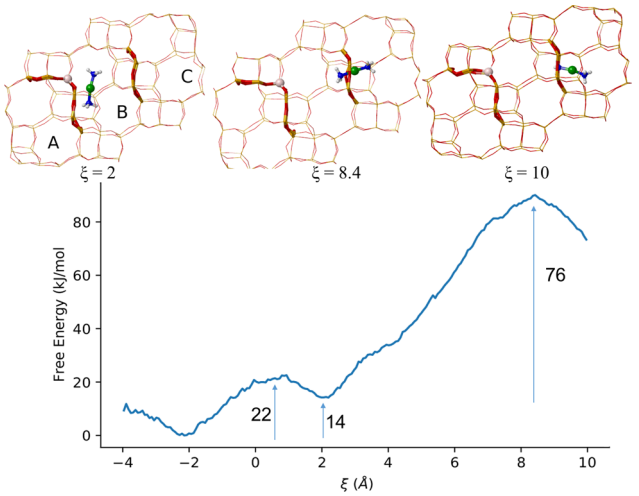

Figure 4. Snapshots of the $[Cu(NH_3)_2]^+$ diffusion path through multiple 8-ring windows of CHA and corresponding free energy profile at 423 K. Si and O atoms in the framework are depicted as yellow and red sticks; Al, Cu, N, and H atoms are depicted as thatch, green, blue, and white balls, respectively.

temperature, method, and collective variable used in both simulations, our results point to the same qualitative conclusion, namely, that for $[Cu(NH_3)_2]^+$ complexes, only migration between two cavities A and B sharing an Al atom is energetically feasible. Therefore, the rest of the diffusion study was performed using the 1 × 1 × 1 unit cell described in the computational details section.

The presence of another $[Cu(NH_3)_2]^+$ complex in cavity B, which is mandatory to form dimers, raises the diffusion free energy barrier to 28 kJ/mol and makes the process endothermic by 7 kJ/mol (case *II* in Table 1 and Figures 2 and 3). This destabilization is probably due to an electrostatic effect, since both positively charged Cu^+ cations are closer in the final state. An additional O_2 molecule in cavity B (case *III*) or even 2NO + O_2 in cavity B (case *IV*) has an almost negligible influence on activation and reaction free energies (see Table 1 and Figure 3), suggesting a low contribution of entropic effects associated with too crowded cavities. Moreover, formation of the proposed transient dimeric $Cu(NH_3)_2$-O_2-$Cu(NH_3)_2$ species occurs spontaneously when the two $[Cu(NH_3)_2]^+$ monomers and O_2 occupy the same cavity (case *III*), but it does not lead to any additional stabilization of the system. Thus, at 423 K and in the presence of the reactants involved in the oxidation half-cycle of the mechanism, the movement of the $[Cu(NH_3)_2]^+$ complex to an adjacent occupied cavity appears to occur relatively easy, as indicated by the blue, yellow, green and red free energy profiles in Figure 3. Notice that despite no additional walls were imposed to restrict the movement or diffusion of NO and O_2, these molecules always remained in their original cavity during the simulations.

Next, we considered the possible influence of the reactant NH_3 and the product water that are always present under reaction conditions. Both molecules can form relatively strong hydrogen bonds with the NH_3 ligands attached to Cu^+ and with the framework O atoms, which might hinder the mobility of the $[Cu(NH_3)_2]^+$ complexes and their diffusion through the 8-ring windows. The activation barriers obtained for these two cases (*V* and *VI* in Table 1 and Figures 3 and 5) are similar to those described so far, but the final states are less stable by 10 and 15 kJ/mol for water and ammonia, respectively. This is probably due to the loss of some stabilizing interactions between the $[Cu(NH_3)_2]^+$ complex and the water or NH_3 molecules that remain in the initial cavity. Since the influence of NH_3 seems to be larger than that of water and in order to bring some light into the NH_3 inhibition effect previously described, the two NH_3 molecules were initially placed in cavity A and the diffusion to an empty cavity B was studied (case *VII* in Table 1 and Figures 3 and 5). In this case, the stabilization of the $[Cu(NH_3)_2]^+$ species through hydrogen bonds in cavity A is more evident, and both activation and reaction free energies increase significantly to 47 and 36 kJ/mol, respectively (see Table 1 and Figure 3, pink line). Comparison of these values with those obtained from the simulation represented in Figure 2, case *II*, with a similar final state in cavity B, indicates that the much larger activation and reaction free energy values obtained in the presence of NH_3 are due to the higher stability of the initial state. After diffusion of the $[Cu(NH_3)_2]^+$ complex to cavity B, the two additional NH_3 molecules remain in the initial cavity A (see Figure 5). The detachment of the two NH_3 molecules from the $[Cu(NH_3)_2]^+$ complex in the transition state and in the final state results in the loss of some stabilizing interactions that were present in the initial state, thus explaining the higher activation and reaction energies. The NH_3 inhibition effect on the SCR reaction identified by *in situ* and *operando* XAS studies combined with catalytic activity tests at low temperature was attributed to a decrease in the rate of the oxidation of Cu^+ to Cu^{2+} in excess of NH_3.[26,27,29,30] The difficult diffusion of the $[Cu(NH_3)_2]^+(NH_3)_2$ species described here would hinder the formation of the $Cu(NH_3)_2$-O_2-$Cu(NH_3)_2$ dimers necessary for the oxidation step at low temperature, thus explaining the experimental observations.

The same negative effect on mobility is observed when two NO molecules are introduced in cavity A and interact with the Cu^+ cation, forming a stable and bulky $[Cu(NH_3)_2]^+(NO)_2$ complex (see Figure 5, case *VIII*). The activation and reaction free energies obtained from the simulations are 54 and 34 kJ/mol, respectively (see Table 1 and Figure 3, gray line) and reflect the energy penalty associated with the dissociation of the bonds between Cu^+ and the NO molecules, necessary for the $[Cu(NH_3)_2]^+$ complex to cross the 8-ring. The high barriers for diffusion found here are in agreement with the mass transport limitations of NH_3 and NO reported by Becher et al. during NH3-SCR-NOx reaction using a Cu-SSZ-13 catalyst.[30] To further clarify this point, we explored in more detail the interaction of Cu^+ with 2NO and 2NH_3 molecules, as this equimolar NO:NH_3 ratio is one of the reactant compositions most widely used in *operando* studies of copper speciation and reaction mechanism.[22,23,26−30]

3.2. Stability of $[Cu(NH_3)_2]^+(NO)_x$ and Interaction with O_2

Taking Cu^+ placed in the 6-ring of Cu-CHA zeolite and the two NO and two NH_3 molecules free in the center of the CHA cavity (see Figure S7a) as the starting point, regular AIMD simulations were run at 298, 523, and 673 K to cover both low and high temperature regimes. At the three temperatures considered, the two NH_3 molecules bind to Cu^+ and detach it from the 6-ring, with average distances between the Cu^+ cation and the 6-ring plane larger than 3.5 Å in all cases (see *d* Cu-6r in Table 2). A $[Cu(NH_3)_2]^+(NO)$ species is observed at 298 K, while the $[Cu(NH_3)_2]^+(NO)_2$ complex is formed at 523 and 673 K (see Figure 6a). The time evolution of the Cu−N1

https://doi.org/10.1021/jacsau.1c00337
JACS Au 2021, 1, 1778−1787

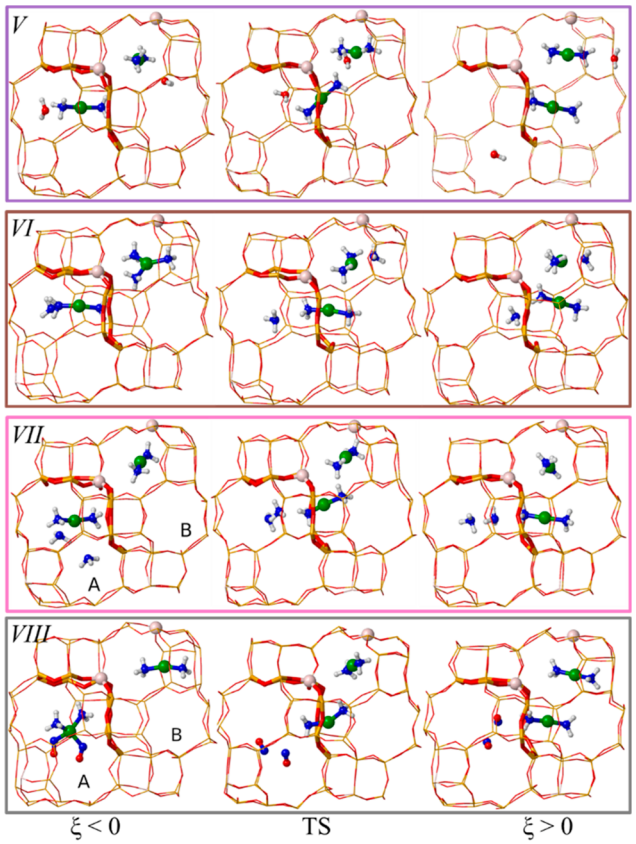

Figure 5. Snapshots of initial ($\xi < 0$), transition state (TS) and final state ($\xi > 0$) of $[Cu(NH_3)_2]^+$ diffusion through the 8-ring windows of Cu-CHA at 423 K in the presence of water, NH_3 and NH_3+NO. Si and O atoms in the framework are depicted as yellow and red sticks; Al, Cu, O in molecules and N and H atoms are depicted as thatch, green, red, blue, and white balls, respectively.

Table 2. Average Distances (d) in Å between Cu^+ and N Atom of Two NO Molecules (Cu−N1 and Cu−N2), between Cu^+ and Average Plane of 6r (Cu-6r), between N atoms of Two NO Molecules and O_2 Molecule (N1−O1 and N2−O2), and between Both O Atoms of O_2[a]

	Cu-CHA + 2NO			Cu-CHA + 2NO+O_2		
T(K)	298	523	673	298	523	673
d Cu−N1	1.94	2.20	2.37	4.11	4.97	4.15
d Cu−N2	3.29	2.17	2.64	2.86	4.90	3.75
d Cu-6r	3.87	6.10	4.01	3.60	3.20	3.28
d N1−O1				2.27	1.84	1.48
d N2−O2				2.66	1.79	1.38
d O1−O2				1.30	1.36	3.76

[a]The atom labeling is shown in Figure 6.

and Cu−N2 distances in Figure S8 in the SI indicate that the interaction of the $[Cu(NH_3)_2]^+$ complex with the two NO molecules is relatively strong. At 298 K, one NO coordinates to Cu^+ with an average bond length of 1.94 Å, while the other NO remains at 3.3 Å from Cu^+. At 523 and 673 K, both NO coordinate to Cu^+ with average bond lengths of 1.97 Å and remain bonded to the cationic site most of the time. A completely different picture is obtained when O_2 is introduced in the system (Figures S7b and 6b). The presence of O_2 weakens the interaction of NO with the $[Cu(NH_3)_2]^+$ complex, with at most one NO molecule being bonded to

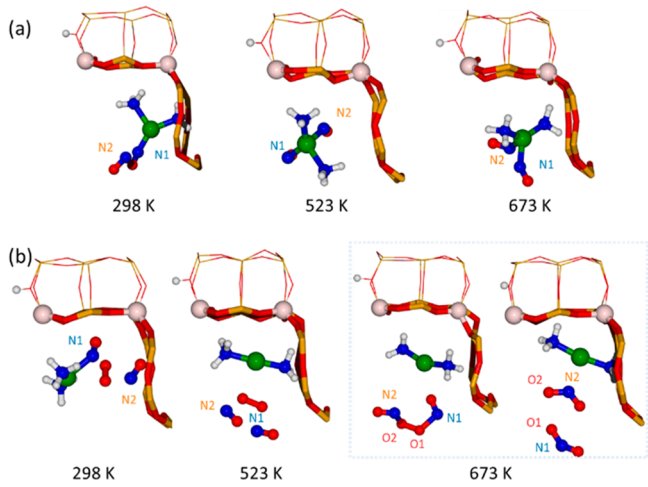

Figure 6. Snapshots of the interaction of Cu^+ with (a) 2NO + $2NH_3$ and (b) 2NO + $2NH_3$ + O_2 in Cu-CHA at 298, 523, and 673 K. Si and O atoms in the framework are depicted as yellow and red sticks; Al, Cu, O in molecules and N and H atoms are depicted as thatch, green, red, blue, and white balls, respectively.

Cu^+ at 298 K, and the system becomes more dynamic. The time evolution of the Cu−N1 and Cu−N2 distances in Figure S9 evidence that at 523 K, the two NO molecules are most of the time at ∼5 Å from Cu^+. Also, the average intermolecular distances N1−O1 and N2−O2 (Figure 6b) are 1.84 and 1.79 Å respectively, which shows that there is a favorable interaction between the NO molecules and O_2 (see Table 2). At around 40 ps, the $[Cu(NH_3)_2]^+$ complex diffuses through the 8-ring to the neighboring cavity and remains there for about 8 ps before returning the initial cavity. This results in a temporary increase of Cu−N1 and Cu−N2 distances to ∼10 Å, since O_2 and the two NO molecules remain in the initial cavity during the whole simulation. The spontaneous diffusion of the $[Cu(NH_3)_2]^+$ species at 523 K can be observed in the scatterplot of the Cu^+ cation trajectory shown in Figure 7.

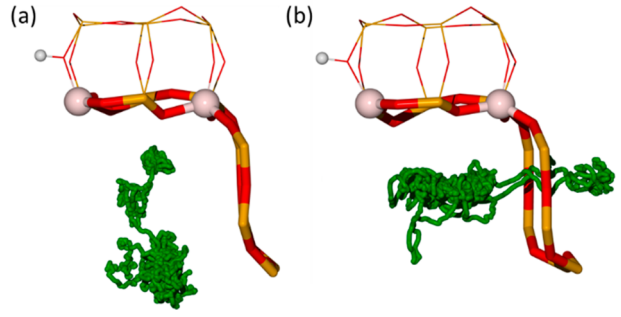

Figure 7. Scatter plot of the position of Cu^+ along the trajectory of an AIMD simulation of the interaction of Cu^+ with (a) 2NO + $2NH_3$ and (b) 2NO + $2NH_3$ + O_2 in Cu-CHA at 523 K. For clarity, the positions of the NO, NH_3, and O_2 molecules are omitted.

These results evidence that the detachment of the NO molecules from the bulky $[Cu(NH_3)_2]^+(NO)_2$ complex due to the presence of O_2 in the cavity facilitates its diffusion through the 8-ring window, due to a decrease in the activation free energy barrier from 54 kJ/mol to ∼20−24 kJ/mol (see Table 1).

Interestingly, at 673 K, the spontaneous dissociation of the O−O bond of the O_2 molecule and the consequent formation

https://doi.org/10.1021/jacsau.1c00337
JACS Au 2021, 1, 1778−1787

of two NO_2 molecules is observed after 12 ps of simulation (see Figure S4). During the transition, neither O_2 nor NO are bonded to Cu^+. The three molecules interact with each other (see Figure 6b), and the rupture of the O−O bond and the formation of the two new N−O bonds occur simultaneously. Furthermore, the Cu−N2 distance decreases to ∼2.0 Å at around 13 ps, indicating that one of the NO_2 molecules coordinates to Cu^+ after the reaction. The reverse event did not happen and at least one of the two NO_2 molecules formed remained attached to Cu^+ during the rest of the simulation. This finding agrees with the proposal that the global SCR reaction rate increases significantly in the high temperature regime, that is, at $T > 623$ K, due to the contribution of the fast SCR cycle, because NO_2 production by direct NO oxidation with O_2 is enhanced at this temperature.[26,27,29,33]

3.3. Reaction path for NO oxidation to NO_2

At this point, the interaction of an O_2 molecule with the stable $[Cu(NH_3)_2(NO)_2]^+$ complex and the reaction path to form two NO_2 molecules were studied by means of AI-US simulations in order to get an estimation of the activation energy necessary to oxidize NO. These AI-US simulations are biased along a collective variable, CN_{OX}, which represents the simultaneous dissociation of the O−O bond and the formation of two new N−O bonds as depicted in Figure 1c (see Computational Details). Since spontaneous O−O dissociation and NO_2 formation were observed in the regular AIMD simulations at 673 K, the investigation of the reaction path using enhanced techniques was done at a lower temperature of 423 K. The free energy profile for this process at 423 K is shown in Figure 8, where the labels A, B, and C correspond to

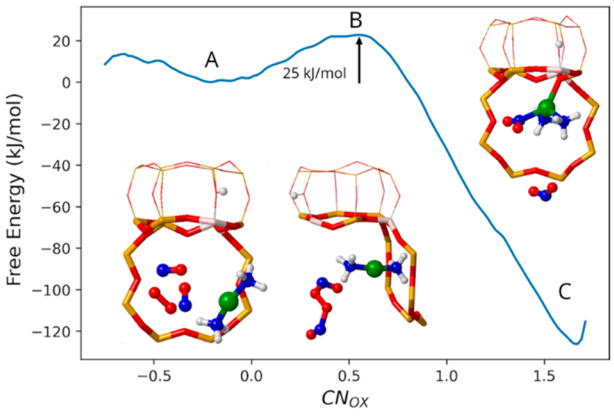

Figure 8. Free energy profile for the oxidation of NO with O_2 in the presence of the $[Cu(NH_3)_2]^+$ complex in the CHA cavity from ab initio umbrella sampling AI-US simulations at 423 K. Snapshots of reactants (A), transition state (B), and products (C) are included in the plot.

the reactants, transition state, and products, respectively. In accordance with the results from regular AIMD, the two NO and O_2 molecules interact with each other more strongly than with Cu^+ so that they are, on average, more than 2.6 Å away from Cu^+ during the whole process. In the transition state, the two new N−O bonds are formed as the O−O bond breaks, and only after the reaction has happened one of the NO_2 molecules starts interacting with the Cu^+ cation. The low value obtained for the activation free energy barrier, ∼25 kJ/mol, indicates that the oxidation of NO with O_2 inside the CHA cage to generate NO_2 is an easy process, and that the subsequent interaction of this NO_2 with Cu^+ might produce its rapid oxidation to Cu^{2+}. This additional pathway for Cu^+ oxidation to Cu^{2+} at low temperature without requiring the formation of $Cu(NH_3)_2$-O_2-$Cu(NH_3)_2$ dimers would explain recent *in situ* UV−vis results showing a promoting effect of both NO and NO_2 on the $Cu^+ \rightarrow Cu^{2+}$ oxidation step in Cu-CHA zeolites at 473 K.[28]

4. CONCLUSION

In summary, AIMD simulations show that the diffusion of an isolated $[Cu(NH_3)_2]^+$ complex through the 8-ring windows of the CHA structure is relatively easy, and the free energy profile is not altered too much by the presence of another $[Cu(NH_3)_2]^+$ monomer or additional molecules in the final cavity B. In contrast, diffusion is significantly hindered when reactant molecules, in particular, NH_3 and NO, are present in the initial cavity A. NH_3 forms hydrogen bonds with the ligands of the complex and with the framework O atoms, while NO binds to the central Cu^+ atom of the complex. In both cases, the stable intermediates formed are too bulky to cross the 8-ring window, and the necessary decoordination of the additional ligands involves an energy penalty reflected in higher activation and reaction free energies. Therefore, the local concentration of some particular reactants in the close environment of the copper active sites is identified as a key factor strongly influencing the mobility of $[Cu(NH_3)_2]^+$ species at low temperatures. Both the NH_3 inhibition effect previously reported by different groups[26,27,29,30] and transport limitations of NO and NH_3 described recently[30] can be understood in light of these AIMD simulations.

The presence of O_2 in the reaction media strongly modifies the interaction of NO with Cu^+. At low temperatures ($T \leq 523$ K), O_2 interacts with NO detaching it from the stable $[Cu(NH_3)_2(NO)_2]^+$ complex formed under reducing conditions, thus facilitating the migration of the resulting $[Cu(NH_3)_2]^+$ species through the 8-ring windows of CHA to form the dimers involved in the oxidation step. At high temperatures ($T = 673$ K), O_2 reacts spontaneously with the two NO molecules present in the cavity to form two NO_2 molecules, which may oxidize Cu^+ to Cu^{2+} according to the fast SCR reaction, thus enhancing the global SCR reaction rate.[33] These results support the existence of two different reaction mechanisms operating at low and high temperatures, the former involving dimeric $Cu(NH_3)_2$-O_2-$Cu(NH_3)_2$ species and the latter occurring by direct NO oxidation to NO_2 in one single cavity. Moreover, the low activation free energy barrier for NO oxidation to NO_2 obtained from AI-US simulations at 473 K suggests some contribution of this monomer-based pathway to the total NO conversion in the low temperature regime of the SCR reaction, in agreement with recent experimental information.[28] To the best of our knowledge, the present computational approach combining enhanced sampling techniques with ab initio molecular dynamics simulations at operating conditions has not been applied in earlier studies of a complex process such as the NH_3-SCR-NOx reaction. For the first time, we perform operando simulations in the presence of other reactive molecules at low and high temperatures, which enable us to deduce key findings on the reaction mechanism and diffusion in the low and high temperature regimes.

https://doi.org/10.1021/jacsau.1c00337
JACS Au 2021, 1, 1778−1787

■ ASSOCIATED CONTENT

Supporting Information

The Supporting Information is available free of charge at https://pubs.acs.org/doi/10.1021/jacsau.1c00337.

Catalyst models, histograms showing overlap between windows in the US simulations, and time evolution of selected variables during the AIMD simulations (PDF)

■ AUTHOR INFORMATION

Corresponding Authors

Mercedes Boronat − *Instituto de Tecnología Química, Universitat Politècnica de València-Consejo Superior de Investigaciones Científicas, 46022 València, Spain;* orcid.org/0000-0002-6211-5888; Email: boronat@itq.upv.es

Veronique van Speybroeck − *Center for Molecular Modeling, Ghent University, 9052 Zwijnaarde, Belgium;* orcid.org/0000-0003-2206-178X; Email: veronique.vanspeybroeck@ugent.be

Authors

Reisel Millan − *Instituto de Tecnología Química, Universitat Politècnica de València-Consejo Superior de Investigaciones Científicas, 46022 València, Spain;* orcid.org/0000-0002-4489-5411

Pieter Cnudde − *Center for Molecular Modeling, Ghent University, 9052 Zwijnaarde, Belgium;* orcid.org/0000-0002-6735-0078

Complete contact information is available at: https://pubs.acs.org/10.1021/jacsau.1c00337

Author Contributions

The manuscript was written through contributions of all authors. All authors have given approval to the final version of the manuscript.

Funding

Spanish Government through (SEV-2016−0683, MINECO) and MAT2017−82288-C2−1-P (AEI/FEDER, UE). CSIC through the i-link+ program (LINKA20381). European Union's Horizon 2020 research and innovation program through consolidator ERC grant agreement No. 647755 - DYNPOR (2015−2020). Research Foundation - Flanders (FWO).

Notes

The authors declare no competing financial interest.

■ ACKNOWLEDGMENTS

This work has been supported by the Spanish Government through Severo Ochoa (SEV-2016-0683, MINECO), and MAT2017-82288-C2-1-P (AEI/FEDER, UE) projects, and by CSIC through the i-link+ program (LINKA20381). We thankfully acknowledge Red Española de Supercomputación (RES) and Servei d'Informàtica de la Universitat de València (SIUV) for computational resources and technical support, the computer resources at Marenostrum4 (RES-QS-2020-1-0029 and RES-QS.2020-2-0015) and the technical support provided by BSC. R.M. thanks ITQ for his contract. V.V.S, P.C. acknowledge funding from the European Union's Horizon 2020 research and innovation program (consolidator ERC grant agreement No. 647755 - DYNPOR (2015-2020)). V.V.S. acknowledges the Research Board of the Ghent University (BOF). Part of the computational resources and services used were provided by Ghent University (Stevin Supercomputer Infrastructure), the VSC (Flemish Supercomputer Center), funded by the Research Foundation - Flanders (FWO).

■ REFERENCES

(1) Chen, H.-Y. Cu/Zeolite SCR Catalysts for Automotive Diesel NOx Emission Control. In Urea-SCR Technology for deNOx After Treatment of Diesel Exhausts; Nova, I., Tronconi, E., Eds.; *Fundamental and Applied Catalysis*; Springer: New York, NY, 2014; pp 123−147.

(2) Beale, A. M.; Gao, F.; Lezcano-Gonzalez, I.; Peden, C. H. F.; Szanyi, J. Recent Advances in Automotive Catalysis for NOx Emission Control by Small-Pore Microporous Materials. *Chem. Soc. Rev.* **2015**, *44* (20), 7371−7405.

(3) Zhang, R.; Liu, N.; Lei, Z.; Chen, B. Selective Transformation of Various Nitrogen-Containing Exhaust Gases toward N2 over Zeolite Catalysts. *Chem. Rev.* **2016**, *116* (6), 3658−3721.

(4) Kwak, J. H.; Tonkyn, R. G.; Kim, D. H.; Szanyi, J.; Peden, C. H. F. Excellent Activity and Selectivity of Cu-SSZ-13 in the Selective Catalytic Reduction of NOx with NH3. *J. Catal.* **2010**, *275* (2), 187−190.

(5) Gao, F.; Kwak, J. H.; Szanyi, J.; Peden, C. H. F. Current Understanding of Cu-Exchanged Chabazite Molecular Sieves for Use as Commercial Diesel Engine DeNO(x) Catalysts. *Top. Catal.* **2013**, *56* (15−17), 1441−1459.

(6) Martín, N.; Boruntea, R.; Moliner, C.; Corma, M. A. Efficient Synthesis of the Cu-SSZ-39 Catalyst for DeNOx Applications. *Chem. Commun.* **2015**, *51* (55), 11030−11033.

(7) Ryu, T.; Ahn, N. H.; Seo, S.; Cho, J.; Kim, H.; Jo, D.; Park, G. T.; Kim, P. S.; Kim, C. H.; Bruce, E. L.; Wright, P. A.; Nam, I.-S.; Hong, S. B. Fully Copper-Exchanged High-Silica LTA Zeolites as Unrivaled Hydrothermally Stable NH3-SCR Catalysts. *Angew. Chem., Int. Ed.* **2017**, *56* (12), 3256−3260.

(8) Peden, C. H. F. Cu/Chabazite Catalysts for 'Lean-Burn' Vehicle Emission Control. *J. Catal.* **2019**, *373*, 384−389.

(9) Borfecchia, E.; Beato, P.; Svelle, S.; Olsbye, U.; Lamberti, C.; Bordiga, S. Cu-CHA − a Model System for Applied Selective Redox Catalysis. *Chem. Soc. Rev.* **2018**, *47* (22), 8097−8133.

(10) Paolucci, C.; Verma, A. A.; Bates, S. A.; Kispersky, V. F.; Miller, J. T.; Gounder, R.; Delgass, W. N.; Ribeiro, F. H.; Schneider, W. F. Isolation of the Copper Redox Steps in the Standard Selective Catalytic Reduction on Cu-SSZ-13. *Angew. Chem., Int. Ed.* **2014**, *53* (44), 11828−11833.

(11) Janssens, T. V. W.; Falsig, H.; Lundegaard, L. F.; Vennestrom, P. N. R.; Rasmussen, S. B.; Moses, P. G.; Giordanino, F.; Borfecchia, E.; Lomachenko, K. A.; Lamberti, C.; Bordiga, S.; Godiksen, A.; Mossin, S.; Beato, P. A Consistent Reaction Scheme for the Selective Catalytic Reduction of Nitrogen Oxides with Ammonia. *ACS Catal.* **2015**, *5* (5), 2832−2845.

(12) Paolucci, C.; Parekh, A. A.; Khurana, I.; Di Iorio, J. R.; Li, H.; Albarracin Caballero, J. D.; Shih, A. J.; Anggara, T.; Delgass, W. N.; Miller, J. T.; Ribeiro, F. H.; Gounder, R.; Schneider, W. F. Catalysis in a Cage: Condition-Dependent Speciation and Dynamics of Exchanged Cu Cations in SSZ-13 Zeolites. *J. Am. Chem. Soc.* **2016**, *138* (18), 6028−6048.

(13) Gao, F.; Mei, D.; Wang, Y.; Szanyi, J.; Peden, C. H. F. Selective Catalytic Reduction over Cu/SSZ-13: Linking Homo- and Heterogeneous Catalysis. *J. Am. Chem. Soc.* **2017**, *139* (13), 4935−4942.

(14) Paolucci, C.; Khurana, I.; Parekh, A. A.; Li, S.; Shih, A. J.; Li, H.; Iorio, J. R. D.; Albarracin-Caballero, J. D.; Yezerets, A.; Miller, J. T.; Delgass, W. N.; Ribeiro, F. H.; Schneider, W. F.; Gounder, R. Dynamic Multinuclear Sites Formed by Mobilized Copper Ions in NOx Selective Catalytic Reduction. *Science* **2017**, *357* (6354), 898−903.

(15) Moreno-González, M.; Millán, R.; Concepción, P.; Blasco, T.; Boronat, M. Spectroscopic Evidence and Density Functional Theory

(DFT) Analysis of Low-Temperature Oxidation of Cu+ to Cu2+NOx in Cu-CHA Catalysts: Implications for the SCR-NOx Reaction Mechanism. *ACS Catal.* **2019**, *9* (4), 2725−2738.
(16) Jones, C. B.; Khurana, I.; Krishna, S. H.; Shih, A. J.; Delgass, W. N.; Miller, J. T.; Ribeiro, F. H.; Schneider, W. F.; Gounder, R. Effects of Dioxygen Pressure on Rates of NOx Selective Catalytic Reduction with NH3 on Cu-CHA Zeolites. *J. Catal.* **2020**, *389*, 140−149.
(17) Chen, L.; Janssens, T. V. W.; Vennestrøm, P. N. R.; Jansson, J.; Skoglundh, M.; Grönbeck, H. A Complete Multisite Reaction Mechanism for Low-Temperature NH3-SCR over Cu-CHA. *ACS Catal.* **2020**, *10* (10), 5646−5656.
(18) Paolucci, C.; Di Iorio, J. R.; Schneider, W. F.; Gounder, R. Solvation and Mobilization of Copper Active Sites in Zeolites by Ammonia: Consequences for the Catalytic Reduction of Nitrogen Oxides. *Acc. Chem. Res.* **2020**, *53* (9), 1881−1892.
(19) Gao, F.; Washton, N. M.; Wang, Y.; Kollár, M.; Szanyi, J.; Peden, C. H. F. Effects of Si/Al Ratio on Cu/SSZ-13 NH3-SCR Catalysts: Implications for the Active Cu Species and the Roles of Brønsted Acidity. *J. Catal.* **2015**, *331*, 25−38.
(20) Di Iorio, J. R.; Bates, S. A.; Verma, A. A.; Delgass, W. N.; Ribeiro, F. H.; Miller, J. T.; Gounder, R. The Dynamic Nature of Brønsted Acid Sites in Cu−Zeolites During NOx Selective Catalytic Reduction: Quantification by Gas-Phase Ammonia Titration. *Top. Catal.* **2015**, *58* (7), 424−434.
(21) Borfecchia, E.; Lomachenko, K. A.; Giordanino, F.; Falsig, H.; Beato, P.; Soldatov, A. V.; Bordiga, S.; Lamberti, C. Revisiting the Nature of Cu Sites in the Activated Cu-SSZ-13 Catalyst for SCR Reaction. *Chem. Sci.* **2015**, *6* (1), 548−563.
(22) Beale, A. M.; Lezcano-Gonzalez, I.; Slawinksi, W. A.; Wragg, D. S. Correlation between Cu Ion Migration Behaviour and DeNO(x) Activity in Cu-SSZ-13 for the Standard NH3-SCR Reaction. *Chem. Commun.* **2016**, *52* (36), 6170−6173.
(23) Lomachenko, K. A.; Borfecchia, E.; Negri, C.; Berlier, G.; Lamberti, C.; Beato, P.; Falsig, H.; Bordiga, S. The Cu-CHA DeNO(x) Catalyst in Action: Temperature-Dependent NH3-Assisted Selective Catalytic Reduction Monitored by Operando XAS and XES. *J. Am. Chem. Soc.* **2016**, *138* (37), 12025−12028.
(24) Martini, A.; Borfecchia, E.; Lomachenko, K. A.; Pankin, I. A.; Negri, C.; Berlier, G.; Beato, P.; Falsig, H.; Bordiga, S.; Lamberti, C. Composition-Driven Cu-Speciation and Reducibility in Cu-CHA Zeolite Catalysts: A Multivariate XAS/FTIR Approach to Complexity. *Chem. Sci.* **2017**, *8* (10), 6836−6851.
(25) Andersen, C. W.; Borfecchia, E.; Bremholm, M.; Jørgensen, M. R. V.; Vennestrøm, P. N. R.; Lamberti, C.; Lundegaard, L. F.; Iversen, B. B. Redox-Driven Migration of Copper Ions in the Cu-CHA Zeolite as Shown by the In Situ PXRD/XANES Technique. *Angew. Chem., Int. Ed.* **2017**, *56* (35), 10367−10372.
(26) Marberger, A.; Petrov, A. W.; Steiger, P.; Elsener, M.; Kröcher, O.; Nachtegaal, M.; Ferri, D. Time-Resolved Copper Speciation during Selective Catalytic Reduction of NO on Cu-SSZ-13. *Nat. Catal.* **2018**, *1* (3), 221−227.
(27) Fahami, A. R.; Günter, T.; Doronkin, D. E.; Casapu, M.; Zengel, D.; Vuong, T. H.; Simon, M.; Breher, F.; Kucherov, A. V.; Brückner, A.; Grunwaldt, J.-D. The Dynamic Nature of Cu Sites in Cu-SSZ-13 and the Origin of the Seagull NOx Conversion Profile during NH3-SCR. *React. Chem. Eng.* **2019**, *4* (6), 1000−1018.
(28) Liu, C.; Kubota, H.; Amada, T.; Kon, K.; Toyao, T.; Maeno, Z.; Ueda, K.; Ohyama, J.; Satsuma, A.; Tanigawa, T.; Tsunoji, N.; Sano, T.; Shimizu, K. In Situ Spectroscopic Studies on the Redox Cycle of NH3−SCR over Cu−CHA Zeolites. *ChemCatChem* **2020**, *12* (11), 3050−3059.
(29) Clark, A. H.; Nuguid, R. J. G.; Steiger, P.; Marberger, A.; Petrov, A. W.; Ferri, D.; Nachtegaal, M.; Kröcher, O. Selective Catalytic Reduction of NO with NH3 on Cu−SSZ-13: Deciphering the Low and High-Temperature Rate-Limiting Steps by Transient XAS Experiments. *ChemCatChem* **2020**, *12* (5), 1429−1435.
(30) Becher, J.; Sanchez, D. F.; Doronkin, D. E.; Zengel, D.; Meira, D. M.; Pascarelli, S.; Grunwaldt, J.-D.; Sheppard, T. L. Chemical Gradients in Automotive Cu-SSZ-13 Catalysts for NO x Removal Revealed by Operando X-Ray Spectrotomography. *Nat. Catal.* **2021**, *4* (1), 46−53.
(31) Oda, A.; Shionoya, H.; Hotta, Y.; Takewaki, T.; Sawabe, K.; Satsuma, A. Spectroscopic Evidence of Efficient Generation of Dicopper Intermediate in Selective Catalytic Reduction of NO over Cu-Ion-Exchanged Zeolites. *ACS Catal.* **2020**, *10* (20), 12333−12339.
(32) Negri, C.; Selleri, T.; Borfecchia, E.; Martini, A.; Lomachenko, K. A.; Janssens, T. V. W.; Cutini, M.; Bordiga, S.; Berlier, G. Structure and Reactivity of Oxygen-Bridged Diamino Dicopper(II) Complexes in Cu-Ion-Exchanged Chabazite Catalyst for NH3-Mediated Selective Catalytic Reduction. *J. Am. Chem. Soc.* **2020**, *142* (37), 15884−15896.
(33) Joshi, S. Y.; Kumar, A.; Luo, J.; Kamasamudram, K.; Currier, N. W.; Yezerets, A. Combined Experimental and Kinetic Modeling Study of the Bi-Modal NOx Conversion Profile on Commercial Cu-SAPO-34 Catalyst under Standard SCR Conditions. *Appl. Catal., B* **2015**, *165*, 27−35.
(34) Cnudde, P.; Demuynck, R.; Vandenbrande, S.; Waroquier, M.; Sastre, G.; Speybroeck, V. V. Light Olefin Diffusion during the MTO Process on H-SAPO-34: A Complex Interplay of Molecular Factors. *J. Am. Chem. Soc.* **2020**, *142* (13), 6007−6017.
(35) Ferri, P.; Li, C.; Millán, R.; Martínez-Triguero, J.; Moliner, M.; Boronat, M.; Corma, A. Impact of Zeolite Framework Composition and Flexibility on Methanol-To-Olefins Selectivity: Confinement or Diffusion? *Angew. Chem., Int. Ed.* **2020**, *59* (44), 19708−19715.
(36) Cnudde, P.; Redekop, E. A.; Dai, W.; Porcaro, N. G.; Waroquier, M.; Bordiga, S.; Hunger, M.; Li, L.; Olsbye, U.; Speybroeck, V. V. Experimental and Theoretical Evidence for the Promotional Effect of Acid Sites on the Diffusion of Alkenes through Small-Pore Zeolites. *Angew. Chem., Int. Ed.* **2021**, *60* (18), 10016−10022.
(37) Millan, R.; Cnudde, P.; Hoffman, A. E. J.; Lopes, C. W.; Concepción, P.; van Speybroeck, V.; Boronat, M. Theoretical and Spectroscopic Evidence of the Dynamic Nature of Copper Active Sites in Cu-CHA Catalysts under Selective Catalytic Reduction (NH3−SCR−NOx) Conditions. *J. Phys. Chem. Lett.* **2020**, *11* (23), 10060−10066.
(38) Chen, L.; Falsig, H.; Janssens, T. V. W.; Jansson, J.; Skoglundh, M.; Grönbeck, H. Effect of Al-distribution on oxygen activation over Cu−CHA. *Catal. Sci. Technol.* **2018**, *8*, 2131−2136.
(39) VandeVondele, J.; Krack, M.; Mohamed, F.; Parrinello, M.; Chassaing, T.; Hutter, J. Quickstep: Fast and Accurate Density Functional Calculations Using a Mixed Gaussian and Plane Waves Approach. *Comput. Phys. Commun.* **2005**, *167* (2), 103−128.
(40) Zhang, Y.; Yang, W. Comment on "Generalized Gradient Approximation Made Simple. *Phys. Rev. Lett.* **1998**, *80* (4), 890−890.
(41) Grimme, S.; Antony, J.; Ehrlich, S.; Krieg, H. A Consistent and Accurate Ab Initio Parametrization of Density Functional Dispersion Correction (DFT-D) for the 94 Elements H-Pu. *J. Chem. Phys.* **2010**, *132* (15), 154104.
(42) Lippert, G.; Hutter, J.; Parrinello, M. The Gaussian and Augmented-Plane-Wave Density Functional Method for Ab Initio Molecular Dynamics Simulations. *Theor. Chem. Acc.* **1999**, *103* (2), 124−140.
(43) Goedecker, S.; Teter, M.; Hutter, J. Separable Dual-Space Gaussian Pseudopotentials. *Phys. Rev. B: Condens. Matter Mater. Phys.* **1996**, *54* (3), 1703−1710.
(44) Martyna, G. J.; Tobias, D. J.; Klein, M. L. Constant Pressure Molecular Dynamics Algorithms. *J. Chem. Phys.* **1994**, *101* (5), 4177−4189.
(45) Hoover, W. G. Canonical Dynamics: Equilibrium Phase-Space Distributions. *Phys. Rev. A: At., Mol., Opt. Phys.* **1985**, *31* (3), 1695−1697.
(46) Frenkel, D.; Smit, B. *Understanding Molecular Simulation: From Algorithms to Applications*; Elsevier Ltd: London, 2001.
(47) Torrie, G. M.; Valleau, J. P. Nonphysical Sampling Distributions in Monte Carlo Free-Energy Estimation: Umbrella Sampling. *J. Comput. Phys.* **1977**, *23* (2), 187−199.

https://doi.org/10.1021/jacsau.1c00337
JACS Au 2021, 1, 1778−1787

(48) Bailleul, S.; Dedecker, K.; Cnudde, P.; Vanduyfhuys, L.; Waroquier, M.; Van Speybroeck, V. Ab initio enhanced sampling kinetic study on MTO ethene methylation reaction. *J. Catal.* **2020**, *388*, 38−51.
(49) Tribello, G. A.; Bonomi, M.; Branduardi, D.; Camilloni, C.; Bussi, G. PLUMED 2: New Feathers for an Old Bird. *Comput. Phys. Commun.* **2014**, *185* (2), 604−613.
(50) Kumar, S.; Rosenberg, J. M.; Bouzida, D.; Swendsen, R. H.; Kollman, P. A. THE Weighted Histogram Analysis Method for Free-Energy Calculations on Biomolecules. I. The Method. *J. Comput. Chem.* **1992**, *13* (8), 1011−1021.
(51) Souaille, M.; Roux, B. Extension to the Weighted Histogram Analysis Method: Combining Umbrella Sampling with Free Energy Calculations. *Comput. Phys. Commun.* **2001**, *135* (1), 40−57.

https://doi.org/10.1021/jacsau.1c00337
JACS Au 2021, 1, 1778−1787